2nd Advanced Optical Metrology Compendium

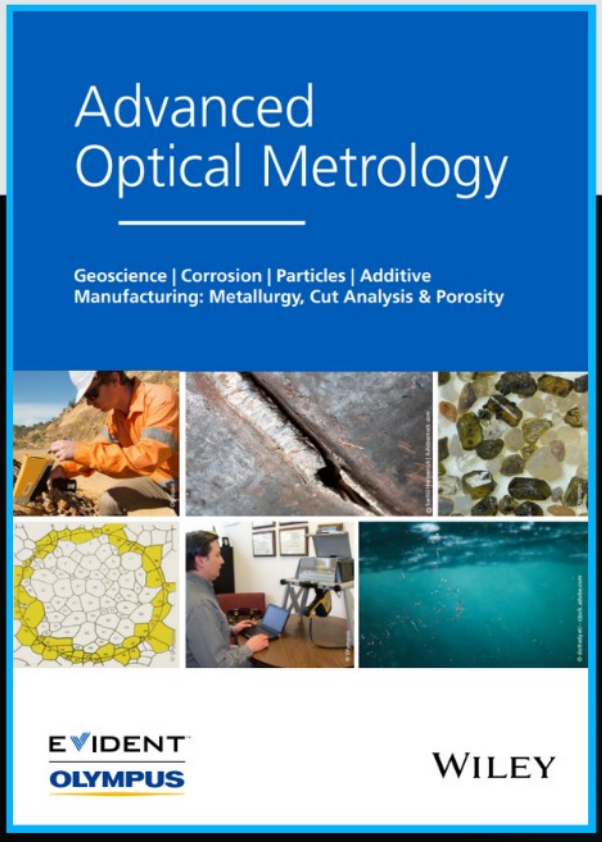

The latest eBook from Advanced Optical Metrology. Download for free.

This compendium includes a collection of optical metrology papers, a repository of teaching materials, and instructions on how to publish scientific achievements.

With the aim of improving communication between fundamental research and industrial applications in the field of optical metrology we have collected and organized existing information and made it more accessible and useful for researchers and practitioners.

EVIDENT
OLYMPUS

WILEY

ADVANCED FUNCTIONAL MATERIALS
www.afm-journal.de

Diameter-Selective Density Enhancement of Horizontally Aligned Single-Walled Carbon Nanotube Arrays by Temperature-Mediated Method

Hongjie Zhang, Wenhuai Zhuge, Feng Yang, Lixing Kang, Shuchen Zhang, Ran Du, Jinjie Qian, Zhi Yang, Yagang Yao, Pan Li, Yue Hu,* and Jin Zhang**

High-density single-walled carbon nanotube (SWNT) arrays with specific diameters are pursued as potential building blocks in future nanoelectronic devices. The direct growth of SWNT arrays on the single-crystal substrate has proved offering densely packing high-quality SWNTs. However, further increase of SWNT density is limited by the deactivation of the catalyst nanoparticles during chemical vapor deposition process. Moreover, an increase of array density without any structure control of SWNTs would make the benefit effect very limited. Here, a temperature-mediated method is proposed to achieve a high-density SWNT array with a specific diameter via continual growth of SWNTs after reactivating poisoned catalysts with high carbon capacity and appropriate size. The density of obtained SWNT array on the quartz substrate is increased by more than three times, with diameter distribution controlled ≈2 nm. This approach paves the way for the integration of SWNTs into nanodevices.

1. Introduction

The application of single-walled carbon nanotube (SWNT) in integrated circuits (ICs) has proposed several key demands on layouts and structures of the nanotube sample, such as electronic property, density, alignment, and diameter of SWNTs.[1] Specially, the degree of density and the alignment should be sufficiently high to fabricate large-scale ICs through industry-compatible technologies[2]; the nanotube diameter should be within a proper range because the requirements on bandgap and the contact resistance at the interface should both be satisfied.[3] Various studies are now being conducted on the synthesis of the desired SWNT arrays using two major approaches, post-synthesis treatment methods, and direct growth methods. The post-synthesis techniques such as multiple transfer techniques,[4] multiple dispersion and sorting process method,[5] soft-lock drawing method,[6] and Langmuir–Schaefer methods[7] have been reported to prepare high-density SWNT arrays promising for IC application, where the orientation, surface cleanness and diameter control of the nanotubes still

H. Zhang, W. Zhuge, J. Qian, Z. Yang, Y. Hu
Key Laboratory of Carbon Materials of Zhejiang Province
College of Chemistry and Materials Engineering
Wenzhou University
Wenzhou 325000, P. R. China
E-mail: yuehu@wzu.edu.cn

F. Yang
Department of Chemistry
Guangdong Provincial Key Laboratory of Catalysis
Southern University of Science and Technology
Shenzhen 518055, P. R. China

L. Kang
Division of Advanced Materials
Suzhou Institute of Nano-Tech and Nano-Bionics
Chinese Academy of Sciences
Suzhou 215123, P. R. China

S. Zhang, J. Zhang
Beijing Science and Engineering Center for Nanocarbons
School of Materials Science and Engineering
College of Chemistry and Molecular Engineering
Peking University
Beijing 100871, P. R. China
E-mail: jinzhang@pku.edu.cn

The ORCID identification number(s) for the author(s) of this article can be found under https://doi.org/10.1002/adfm.202209391.

R. Du
School of materials science & engineering
Beijing Institute of Technology
Beijing 100081, P. R. China

Y. Yao
National Laboratory of Solid State Microstructures
College of Engineering and Applied Sciences
Jiangsu Key Laboratory of Artificial Functional Materials
and Collaborative Innovation Center of Advanced Microstructures
Nanjing University
Nanjing 210093, P.R. China

P. Li
Institute of Advanced Materials
Nanjing University of Posts and Telecommunications
Nanjing 210023, P. R. China
E-mail: iampli@njupt.edu.cn

DOI: 10.1002/adfm.202209391

need to be improved before their practical application. In contrast, direct growth by chemical vapor deposition (CVD) methods has attracted extensive attention because they could produce clean and high-quality horizontal arrays. It is known that the critical factor is the catalyst in direct growth methods.[8] Therefore, the studies aiming at increasing the SWNT arrays density all tried to enhance the efficiency of catalysts from different aspects including magnesium-assisted catalyst anchoring strategy,[9] multiple-cycle growth method,[10] sequential CVD method,[11] multiple catalysts reactivation method,[12] and Trojan catalysts method,[13] which ended up with horizontal arrays density of 20–160 SWNTs μm^{-1}. However, these approaches commonly experience an etching environment, which will invariably influence the quality and structure of the as-grown SWNTs. Meanwhile, the increase in catalyst efficiency was often carried out based on empirical rules, due to the lack of a deep investigation of the underlying mechanism. Additionally, enhancing the density of SWNT arrays without any structure control would limit the effect in the application.[3b]

The creation of horizontal arrays of high-density SWNT with specific diameters requires the development of a revolutionary approach. In this work, we develop a novel temperature-mediated method for the growth of high-density SWNTs with controlled diameter distribution by reactivating the poisoned catalysts. The catalyst reactivation occurred at a temperature (referred to as the reactivation temperature, T_{re}) higher than the growth temperature as shown in **Figure 1**. Since the carbon capacities increase at a higher temperature for high carbon capacity metal,[14] the poisoned metal catalysts become capable of catalyzing SWNT growth by dissolving the coated carbon on the surface at T_{re}, which can be found by in situ dynamic observation in the environmental transmission electron microscope (ETEM). This relation between the carbon dissolution capability of metal catalysts and the reactivation temperature is engineered and utilized to realize the growth of nanotubes with specific structures. After multiple temperature-mediated growths, the denser arrays (60 SWNTs μm^{-1}) with average diameters of 2.13 nm are obtained on the quartz substrate. The field-effect transistors (FET) fabricated on obtained SWNT arrays exhibit a better current carrying capability (317 $\mu A\ \mu m^{-1}$).

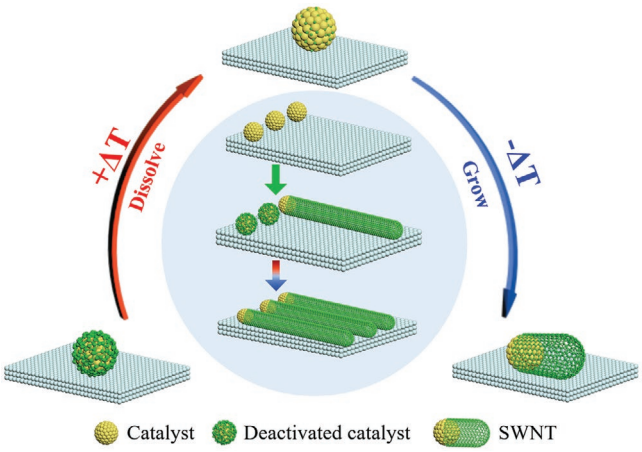

Figure 1. Schematic illustration of growing horizontally aligned SWNT arrays on quartz substrate by the temperature-mediated method.

The temperature-mediated growth strategy realizes the density enhancement of SWNT arrays on quartz, as well as the meaningful structure control. Furthermore, the detailed in situ investigation of the reactivation mechanism is believed to provide essential insights for SWNT growth.

2. Results and Discussion

Herein, iron is used as the metal catalyst for the growth of high-density SWNTs through the temperature-mediated method. From scanning electron microscope (SEM) observations (**Figure 2**a and left image in Figure 2b), uniform high-density SWNT arrays are obtained. Atomic force microscope (AFM) and TEM further indicate that the density of the SWNT arrays can reach 60 SWNTs μm^{-1} in Figure 2b,c. Meanwhile, the high-resolution TEM of SWNT reveals that the obtained SWNTs have a clean and smooth surface, indicating the premium quality of SWNTs. The Raman spectra of the SWNT arrays excited by the 532 nm laser (Figure 2d) are almost free of any D bands, proving the high quality of the SWNT arrays. A narrow distribution ≈2.13 nm of SWNTs diameter can be observed by AFM analysis, which corresponds to the concentrated radial breathing mode (RBM) peak in the Raman spectrum. Hence, the cleanness and orientation of the obtained SWNT arrays are excellent. And the obtained SWNT arrays with high density and specific diameter meet the needs for SWNT applications in nanoelectronics.

According to the vapor–liquid–solid mechanism, the melting point of metal catalysts decreases sharply compared with

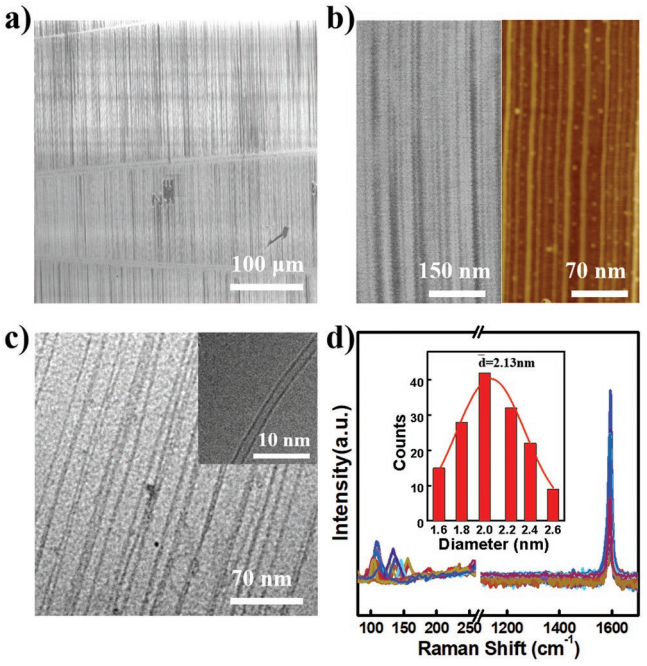

Figure 2. a) SEM images of the high-density SWNTs on a quartz substrate. b) SEM images (left) and AFM images (right) of the high-density SWNTs on a quartz substrate. c) TEM images of the high-density SWNT arrays (Inset: HRTEM image of an individual SWNT). d) Raman spectra of the as-grown SWNTs with 532 nm excitation (Inset: Diameter distribution of the as-grown SWNT arrays).

bulk materials due to the surface interface effect. Hence, the catalyst particles are in a liquid state at a high temperature. The carbon source molecules are decomposed to produce individual carbon atoms on the catalyst's surface and then dissolved into the inner part of metal particles. Carbon atoms are precipitated to nucleate and grow SWNT when the dissolution reaches oversaturation.[15] However, due to the instability of the temperature in the CVD system and the fluctuation of carbon fragment concentration during the process of growing SWNTs, some catalysts may be covered by amorphous carbon, preventing new carbon atoms from being dissolved, which leads to the deactivation of catalyst and the low density of the obtained SWNT arrays. Therefore, how to eliminate the coated carbon of the poisoned catalysts is the key to improving the SWNT array density. According to the metal–carbon phase diagram, the metal has a certain carbon capacity, which could vary with the temperature. Thus, we design a temperature-mediated process to adjust the catalyst's carbon capacity dynamically. In this process, the coated carbon can be dissolved into the catalyst to regrow SWNT and realize high-density horizontal arrays of SWNT. However, the carbon capacity not only varies with temperature but also depends on the size of the metal catalyst.[16] For catalyst nanoparticles with too small a size (<1 nm), their carbon capacity is insufficient to dissolve the coated carbon (Figure S1, Supporting Information) fully. Whereas for metal catalysts with too large size (>3 nm), it is almost impossible to grow SWNTs.[17] Therefore, only metal catalysts of appropriate size can be reactivated to grow SWNTs. In other words, the temperature-mediated growth method could somewhat enrich SWNT diameter.

In situ dynamic observation is an excellent technique to get quantitative data on the shape of catalyst nanoparticles and track the catalytic process. A state-of-the-art ETEM is utilized to observe the reactivation process of a poisoned catalyst ≈2 nm at 930 °C. The catalyst deactivation experiment is detailed in the experimental section. **Figure 3**a–d shows a succession of pictures retrieved from the video. At the moment designated as 0 s, it is found that a deactivated catalyst nanoparticle is covered by coated carbon (Figure 3a). Its thickness is ≈0.3 nm, which means maybe one layer of carbon cover the surface of the catalyst. Form 23 s, the coated carbon begins to dissolve into the catalyst (at the position of the arrow in Figure 3b). At 24 s, the coated carbon disappears (at the position of the arrow in Figure 3c), indicating a partial dissolution. At 25 s, the shell can hardly be observed, which indicates a complete dissolution (Figure 3d). Meanwhile, the schematics in Figure 3a–d model this process of catalyst reactivation. Video S1 (Supporting Information) also exhibits the dynamic dissolution process. To further investigate this process, we perform X-ray photoelectron spectroscopy (XPS) to probe the composition of catalysts. For the Fe 2p spectrum, it can be observed that the peak area of the Fe-C peak (at 708.2 and 721.1 eV)[18] gets larger and larger by comparing the XPS images of original catalysts (Figure S2a, Supporting Information) and the poisoned catalysts (Figure 3e) as well as the reactivated catalysts (Figure 3f), which indicates that the carbon capacity in the catalyst has enhanced. A progressive increase of the Fe-C peak (at 284.0 eV)[16c,19] area can be seen in the C1s spectrum by comparing the XPS images of the above three catalysts (Figure S2b–d, Supporting Information), which is caused by a gradual increase of dissolved carbon in the

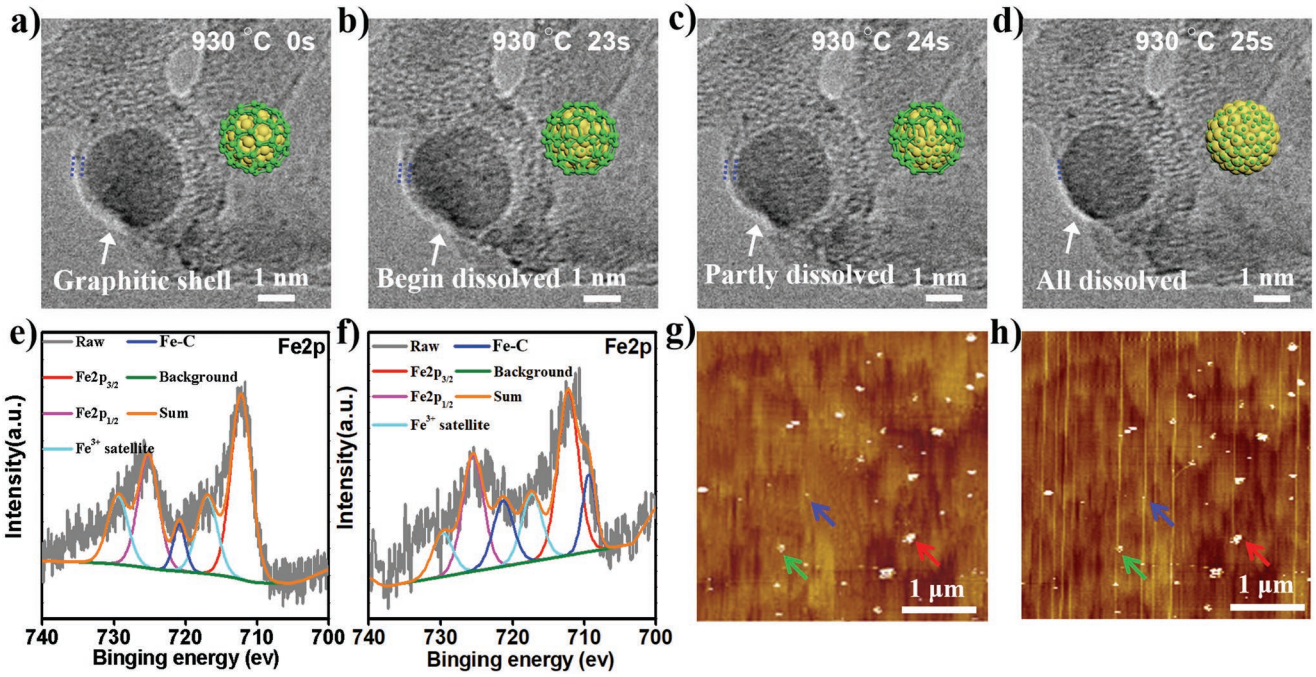

Figure 3. a–d) ETEM images of coated carbon on catalyst nanoparticles surface reactivated at T_{re} (930 °C). e,f) XPS images of deactivated catalyst nanoparticles (e) and reactivated catalyst nanoparticles after maintaining for a while at T_{re} (f). g,h) AFM images of SWNTs obtained from poisoned catalyst nanoparticles after direct growth (g) and temperature-mediated growth (h).

catalyst. This is because the original catalyst contains almost no carbon, and the deactivated catalyst has only a surface layer in contact with the coated carbon. In contrast, carbon can be fully dissolved for the reactivated catalyst, leading to a larger peak area of iron-carbon compounds. Hence, both ETEM and XPS observations indicate that poisoned catalysts can be reactivated by high-temperature processes of the temperature-mediated method. To figure out that the reactivated catalysts can regrow SWNTs, we conduct the experiments on the growth by temperature-mediated method (Temperature-mediated growth involves placing the substrate into the T_{re} position and keeping it for a while, then moving it to the growth temperature position to grow SWNTs). The AFM (Figure 3g) and SEM (Figure S3a, Supporting Information) images show that no SWNT appears when using the poisoned catalysts to grow SWNTs directly. In contrast, several SWNTs emerge (Figure 3h; Figure S3b, Supporting Information) after undergoing a temperature-mediated growth. Consequently, the temperature-mediated method can be used to reactivate the poisoned catalyst to regrow SWNT.

The temperature-mediated method is further used to increase the density of SWNT arrays. We construct direct growth, secondary growth, and temperature-mediated growth by the iron catalyst. SWNT arrays are obtained by direct growth for 2 h (**Figure 4**a). When they undergo secondary growth, the array density remains nearly the same or even decreases (marked by the blue arrow in Figure S4, Supporting Information), which means all catalysts either grow SWNTs or have been deactivated. The disappearance of SWNTs may be caused by hydrogen etching in secondary growth. Afterward, the temperature-mediated growth is performed on this sample and five new SWNTs are found (marked by red arrows in Figure 4b), proving that the temperature-mediated method can increase the array density. The corresponding AFM images also draw the same conclusion (Figure 4c,d; Figure S5, Supporting Information). Meanwhile, the statistical data from 12 experiments with different initial densities all support the fact that the temperature-mediated strategy could enhance array density (Figure 4e).

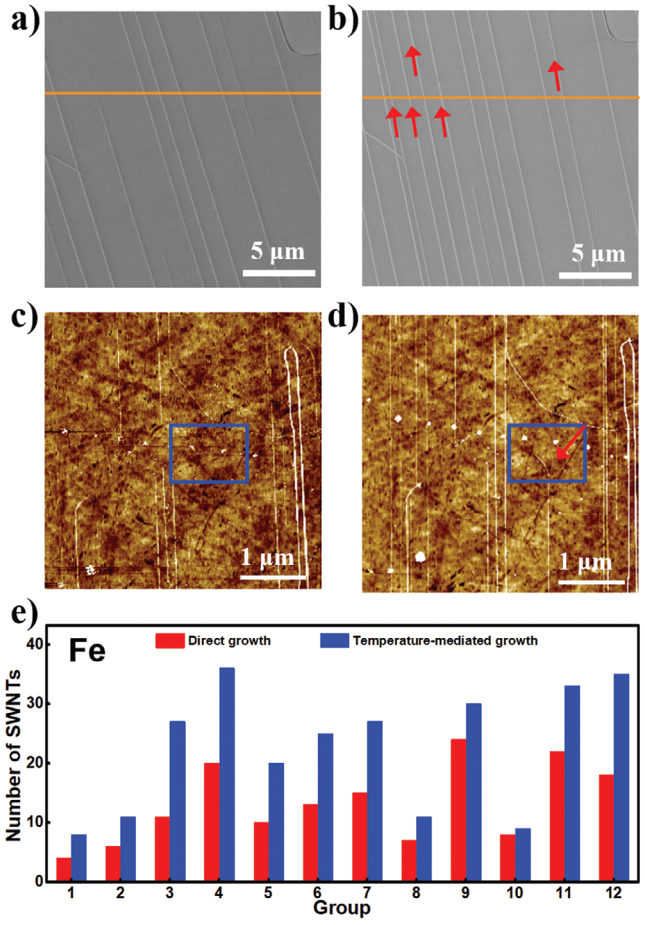

Figure 4. a,b) SEM images of SWNTs after direct growth (a) and the temperature-mediated growth (b) by using Fe catalyst. c,d) AFM images of SWNTs after direct growth (c) and the temperature-mediated growth (d) by using Fe catalyst. e) Statistics of the number of SWNTs by using Fe catalysts within a range of 10 μm × 10 μm.

To obtain denser SWNT arrays, we optimize experimental parameters such as the selection of catalysts, $T_{re,}$ and mediated growth cycles. We analyze the metal-carbon phase diagram to find the optimum metal catalyst. From the metal-carbon phase diagram, the metal could be divided into high-carbon capacity metal and low-carbon capacity metal. For metals with a high carbon capacity, the carbon capacity increases as the temperature rises (Figure S6a, Supporting Information). In contrast, the carbon capacity of metals with a low carbon capacity remains almost the same (Figure S6b, Supporting Information). For high carbon capacity metals such as Fe, Ni, and Co, more SWNTs appear after the temperature-mediated growth (Figure 4; Figures S7 and S8, Supporting Information). But for low carbon capacity metals such as Cu (Figure S9, Supporting Information), Au (Figure S10, Supporting Information), and Ag (Figure S11, Supporting Information), temperature variations have minimal impact on their carbon capacity, resulting in the array density with nearly no change or even reductions. Thus, high carbon capacity metal is chosen for temperature-mediated growth.

The T_{re} selection experiment is then carried out by using Fe catalysts. The growth temperature is set as 830 °C and the T_{re} is chosen from four different temperatures: 830, 880, 930, and 980 °C. When T_{re} is 930 °C, the ratio of increased arrays density can reach ≈167% (**Figure 5**a), which indicates that a temperature difference of 100 °C allows for the greatest increase in catalytic efficiency. The coated carbon may not be dissolved into the catalyst fully at the lower T_{re}, resulting in the poisoned catalyst not being reactivated. At too high T_{re}, catalysts may tend to aggregate and fail to grow SWNTs. Therefore, we choose 930 °C as a proper T_{re} for catalysts reactivation. Then the influence of growth cycles on the array's density is investigated. A growth cycle involves placing the directly grown sample in T_{re} for catalyst reactivation and then placing it at the growth temperature for SWNT growth. As shown in Figure S12 (Supporting Information), we investigate the trends in the number of SWNTs and discover that the tube number continues to rise in the second and third growth cycles while falling in the fourth and fifth growth cycles. Figure 5b shows the statistics of the SWNT numbers over different growth cycles, which indicates that three growth cycles might be the most suitable condition. Using the optimal temperature-mediated method, the density of SWNT

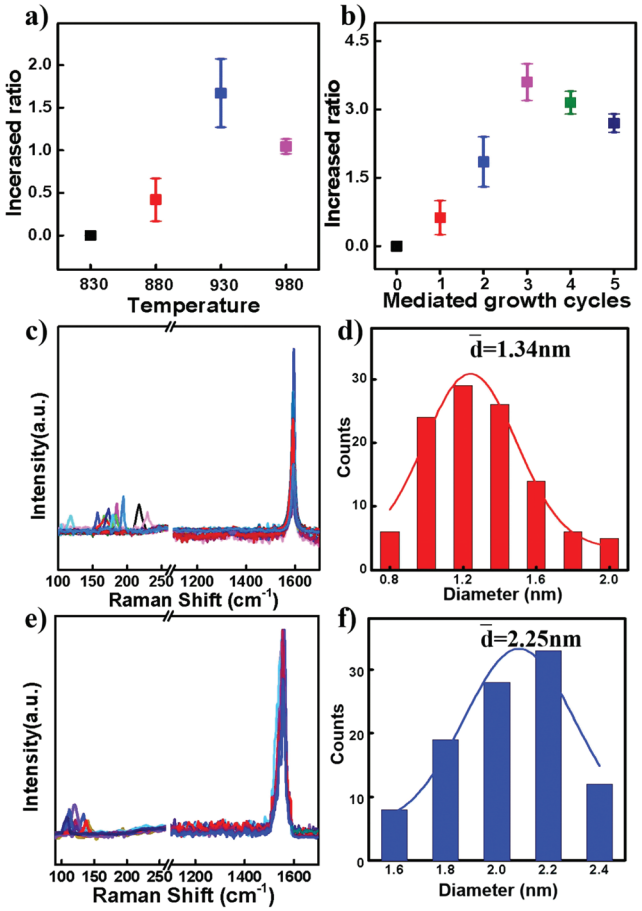

Figure 5. a) The ratio of density enhancement of SWNTs with different T_{re}. b) Statistics of the increased number of SWNTs after different temperature-mediated growth cycles within a range of 10 μm × 10 μm. c,d) Raman spectra (c) and diameter distribution (d) of the SWNT arrays obtained by direct growth with 532 nm excitation. e,f) Raman spectra (e) and diameter distribution (f) of the new SWNT arrays obtained by temperature-mediated growth.

arrays can reach up to 60 SWNTs μm^{-1} (Figure 2). Specially, high-density SWNT arrays are also successfully prepared using Co, Ni catalysts by temperature-mediated method (Figure S13, Supporting Information). Furthermore, this method could also improve SWNT density in the gas flow-guided growth system (Figure S14, Supporting Information).

The ability of the temperature-mediated method to enrich the diameter of SWNTs is further proven. As shown in Figure 5c, for SWNTs obtained by direct growth method, the RBM peaks are randomly distributed in an extensive range (100–250 cm^{-1}), which means that the diameters of SWNTs are uncontrollable. Diameters measured from the AFM image in Figure 4c also proved the wide distribution of array diameters (Figure 5d). But for newly added SWNTs by temperature-mediated growth, the RBM peaks are enriched towards lower Raman shift regions (Figure 5e) and the diameter is concentrated ≈2.25 nm (Figure 5f) by analyzing AFM data in Figure 4d. Besides, Raman spectra of SWNTs with 633 and 785 excitations can reach the same conclusion (Figure S15, Supporting Information). Hence, the temperature-mediated method can enrich the diameter of SWNT arrays, resulting in a horizontal array with a narrow diameter distribution at 2.13 nm as shown in Figure 2, which is more suitable for making high-performance FETs.

Back-gate FET devices are fabricated on the SiO_2/Si substrate with transferred arrays to evaluate the electrical performance of the obtained high-density SWNT arrays. **Figure 6**a,b shows the scheme and optical image of the FET device with a channel width of ≈10 μm and a channel length of ≈2 μm. SWNTs beyond the red box (Figure 6b) are removed by O_2 plasma etching for accurate testing. The arrangement of the SWNTs between electrodes is well arranged as shown in Figure 6c. Figure 6d,e presents the electrical characterization of the fabricated FET devices, in which the largest on-state current could reach 317 μA μm^{-1} at V_{ds} = 1 V. It is benchmarked with previously published work to justify the high performance of our FET device as shown in Figure S16 (Supporting Information). Due to the difference in SWNT array density and nanotube numbers in the channel for different works, we calculate the on-current that a single carbon nanotube could carry in these works (Figure 6f), and it can be found that the performance of our SWNT is excellent. This outstanding performance is due to the obtained SWNT with high quality and appropriate diameter, showing the potential in the application of nanoelectronic devices.

3. Conclusion

In conclusion, a simple and novel method to grow diameter-selective high-density SWNT arrays has been devised. The temperature-mediated method successfully reactivates the poisoned catalysts of a particular size to regrow SWNTs. The density of the obtained SWNT arrays can reach 60 SWNTs μm^{-1}, favoring enrichment of nanotubes with a diameter of ≈2 nm. The largest on-state current of fabricated FETs is 317 μA μm^{-1}, proving the superiority of obtained SWNT arrays. This work is of significant importance for producing SWNT arrays and promoting the application of SWNT-based nanoelectronic devices.

4. Experimental Section

Growth Substrate Preparation: In particular, ST-cut quartz substrates (miscut angle < 0.5°) were purchased from Hefei Kejing Materials Technology Co., China. Samples were obtained by cutting the substrates into smaller pieces (5 mm × 6 mm). These samples were cleaned by ultrasonication in water, acetone, ethanol, and water for 10 min. After cleaning, the substrates must undergo a necessary annealing process (at 900 °C in air for 8 h) for better crystallization.

Catalyst Deactivation Experiment: $Fe(OH)_3$/ethanol solution (0.05 mM), used as a catalyst, was loaded onto the quartz substrates. The CVD growth process was performed in a furnace with a 1-inch tube. The substrates were put into the tube and heated in air to the desired temperature (830 °C). After the system was purged with 300 sccm argon, a flow of hydrogen (100 sccm) was introduced for 10 min to reduce the catalysts. Then additional argon (500 sccm, through an ethanol bubbler) was introduced. The instantaneous influx of a large carbon source might completely deactivate the catalyst by covering it with amorphous carbon.

Statistic Experiment of Increasing the Density of SWNT Arrays: Direct growth experiments on 12 pieces of the quartz substrate were performed.

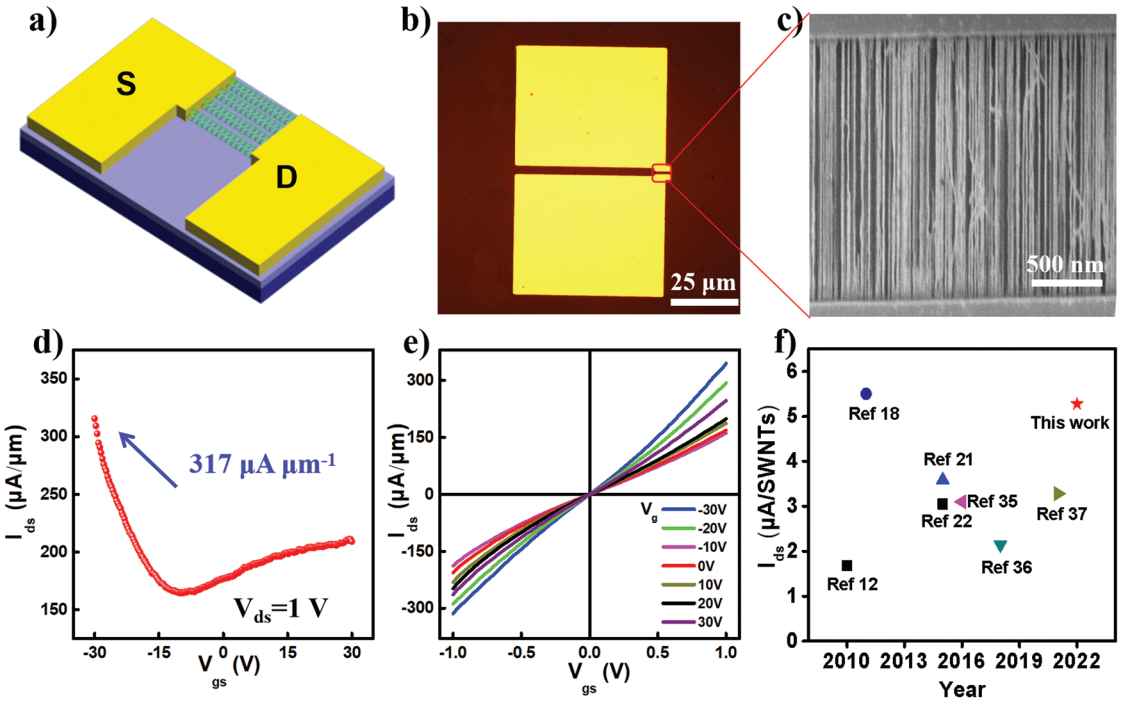

Figure 6. a) Schematic layout of a FET device with a channel length of ≈2 μm and a width of ≈10 μm. Cr (5 nm)/Au (40 nm) are used as contact metals. b) the photo image of the device. c) Corresponding SEM image of SWNT arrays in the red rectangle of (b). d,e) Transfer characteristics (d) and output characteristics (e) of the FET device. f) The on-state current carried by a single SWNT of FET devices is plotted versus the year for the work.[4,8,10,13,20]

Then they were characterized and localized by SEM. Temperature-mediated experiments were then performed, and SEM characterization was conducted in the above-localized area. The number of changes in the density of SWNT arrays in the same range (10 μm × 10 μm) was calculated before and after the temperature-mediated growth on each quartz. Twelve sets of data with different initial densities were plotted as a statistical graph.

T_{re} Selection Experiment: Direct growth was first performed at 830 °C on quartz substrates, characterized, and localized by SEM. And then temperature-mediated growth was performed, and the above-localized areas were characterized by SEM again. The T_{re} of temperature-mediated growth was chosen from four different temperatures: 830, 880, 930, and 980 °C. The number of obtained SWNTs was counted respectively. Multiple direct growth and temperature-mediated growth experiments were performed to obtain the statistical result. The ratio of increase in density of SWNT arrays after temperature-mediated growth to direct growth was plotted.

Synthesis of High-Density SWNT Arrays with Diameter Selectivity: The temperature-mediated growth method involved the growth of SWNTs by periodically moving the ST-cut quartz from the growth temperature location to a higher temperature location while the other parameters were identical to those in normal CVD. In the experiment, a 5 mm × 6 mm quartz (Hefei Kejing Materials Technology Company, China) was used as a substrate for the growth of SWNT arrays. And catalyst was one of Fe, Co, and Ni. The catalyst (0.05 mmol L^{-1} solutions of catalyst salts in alcohol) was loaded onto the quartz surface. The growth of SWNT was carried out in a furnace with a 1-inch tube. The furnace was heated to 930 °C and the substrate was placed at the location with a temperature of 830 °C. First, 300 sccm argon and 300 sccm H_2 were introduced for 10 min to reduce the catalysts. Secondly, 30 sccm Ar was bubbled through ethanol (99.5%, Aladdin) for 5 min to grow the SWNT arrays. Subsequently, in an Ar atmosphere, a quartz tube was pushed to drive the substrate to place where the temperature is 930 °C. After 60 s, quartz tube was pushed to drive the substrate return to the location, that is, 830 °C. And then H_2 and 30 sccm Ar were bubbled through ethanol (99.5%, Aladdin) was introduced to grow for 5 min, and then turned off carbon source and H_2. The temperature-mediated cycle was performed three times. Finally, the temperature would drop in an Ar atmosphere.

Characterization of the Obtained SWNT Arrays: The as-grown SWNTs were inspected with SEM (Nova 200 NanoSEM, America, operated at 1.0 kV), tapping-mode AFM (Nano-Scope IIIa, Veeco Co., USA), TEM (The JEOL JEM2100F microscope at 200 kV), and a Raman spectrometer (Renishaw in via, England).

Fabrication of the Devices Based on SWNT Arrays: SWNT arrays were transferred onto a silicon wafer with a 300 nm SiO_2 layer before the fabrication of devices following a published procedure. The devices were patterned by a standard e-beam lithography (EBL) process. Cr (4 nm)/Au (60 nm) were deposited by e-beam evaporation, followed by a lift-off process to form contact electrodes. Another EBL process and O_2 plasma etching were used to remove the SWNTs outside the device channel region. A Si back-gate was used for measuring the performances of FETs. A Keithley 4200-SCS semiconductor characterization system was used for measuring the electrical characteristics.

Supporting Information

Supporting Information is available from the Wiley Online Library or from the author.

Acknowledgements

This work was financially supported by the National Natural Science Foundation of China (51972237, 51802161), Natural Science Foundation of Zhejiang Province (LY19E020008), Basic Science and Technology Research Project of Wenzhou (G20190001), and the State Key Laboratory from Structural Chemistry, Chinese Academy of Sciences (20200015).

Conflict of Interest

The authors declare no conflict of interest.

Data Availability Statement

The data that support the findings of this study are available from the corresponding author upon reasonable request.

Keywords

devices, diameter selectivities, high densities, single-walled carbon nanotubes, temperature-mediated methods

Received: August 14, 2022
Revised: September 13, 2022
Published online: October 10, 2022

[1] a) M. F. L. De Volder, S. H. Tawfick, R. H. Baughman, A. J. Hart, *Science* **2013**, *339*, 535; b) F. Zhang, P.-X. Hou, C. Liu, B.-W. Wang, H. Jiang, M.-L. Chen, D.-M. Sun, J.-C. Li, H.-T. Cong, E. I. Kauppinen, H.-M. Cheng, *Nat. Commun.* **2016**, *7*, 11160; c) F. Wang, D. Yang, L. Li, Y. Liu, X. Wei, W. Zhou, H. Kataura, H. Liu, S. Xie, *Adv. Funct. Mater.* **2021**, *32*, 2107489; d) A. D. Franklin, *Nature* **2013**, *498*, 443; e) X. Wang, M. He, F. Ding, *Mater. Today* **2018**, *21*, 845; f) M. He, S. Zhang, Q. Wu, H. Xue, B. Xin, D. Wang, J. Zhang, *Adv. Mater.* **2019**, *31*, 1800805.

[2] a) X. Yang, T. Liu, R. Li, X. Yang, M. Lyu, L. Fang, L. Zhang, K. Wang, A. Zhu, L. Zhang, C. Qiu, Y.-Z. Zhang, X. Wang, L.-M. Peng, F. Yang, Y. Li, *J. Am. Chem. Soc.* **2021**, *143*, 10120; b) M. Zhao, Y. Chen, K. Wang, Z. Zhang, J. K. Streit, J. A. Fagan, J. Tang, M. Zheng, C. Yang, Z. Zhu, W. Sun, *Science* **2020**, *368*, 878; c) G. Hills, C. Lau, A. Wright, S. Fuller, M. D. Bishop, T. Srimani, P. Kanhaiya, R. Ho, A. Amer, Y. Stein, D. Murphy, Arvind, A. Chandrakasan, M. M. Shulaker, *Nature* **2019**, *572*, 595; d) C. Qiu, Z. Zhang, M. Xiao, Y. Yang, D. Zhong, L.-M. Peng, *Science* **2017**, *355*, 271; e) K. Otsuka, T. Inoue, E. Maeda, R. Kometani, S. Chiashi, S. Maruyama, *ACS Nano* **2017**, *11*, 11497; f) M. He, S. Zhang, J. Zhang, *Chem. Rev.* **2020**, *120*, 12592; g) L. Qian, Y. Xie, M. Zou, J. Zhang, *J. Am. Chem. Soc.* **2021**, *143*, 18805.

[3] a) B. Yu, C. Liu, P.-X. Hou, Y. Tian, S. Li, B. Liu, F. Li, E. I. Kauppinen, H.-M. Cheng, *J. Am. Chem. Soc.* **2011**, *133*, 5232; b) Y.-C. Tseng, K. Phoa, D. Carlton, J. Bokor, *Nano Lett.* **2006**, *6*, 1364.

[4] C. Wang, K. Ryu, L. G. De Arco, A. Badmaev, J. Zhang, X. Lin, Y. Che, C. Zhou, *Nano Res.* **2010**, *3*, 831.

[5] L. Liu, J. Han, L. Xu, J. Zhou, C. Zhao, S. Ding, H. Shi, M. Xiao, L. Ding, Z. Ma, C. Jin, Z. Zhang, L.-M. Peng, *Science* **2020**, *368*, 850.

[6] Y. Guo, E. Shi, J. Zhu, P.-C. Shen, J. Wang, Y. Lin, Y. Mao, S. Deng, B. Li, J.-H. Park, A.-Y. Lu, S. Zhang, Q. Ji, Z. Li, C. Qiu, S. Qiu, Q. Li, L. Dou, Y. Wu, J. Zhang, T. Palacios, A. Cao, J. Kong, *Nat. Nanotechnol.* **2022**, *17*, 278.

[7] Q. Cao, S. J. Han, G. S. Tulevski, Y. Zhu, D. D. Lu, W. Haensch, *Nat. Nanotechnol.* **2013**, *8*, 180.

[8] Y. Hu, H. Zhang, S. Zhang, C. He, Y. Wang, T. Wang, R. Du, J. Qian, P. Li, J. Zhang, *Small* **2021**, *17*, 2103433.

[9] Y. Xie, L. Qian, D. Lin, Y. Yu, S. Wang, J. Zhang, *Angew Chem Int Ed Engl* **2021**, *60*, 9330.

[10] W. Zhou, L. Ding, S. Yang, J. Liu, *ACS Nano* **2011**, *5*, 3849.

[11] S. W. Hong, T. Banks, J. A. Rogers, *Adv. Mater.* **2010**, *22*, 1826.

[12] Z. Wang, Q. Zhao, J. Zhang, *J. Phys. Chem. C* **2018**, *122*, 24823.

[13] a) L. Kang, Y. Hu, H. Zhong, J. Si, S. Zhang, Q. Zhao, J. Lin, Q. Li, Z. Zhang, L. Peng, J. Zhang, *Nano Res.* **2015**, *8*, 3694; b) Y. Hu, L. Kang, Q. Zhao, H. Zhong, S. Zhang, L. Yang, Z. Wang, J. Lin, Q. Li, Z. Zhang, L. Peng, Z. Liu, J. Zhang, *Nat. Commun.* **2015**, *6*, 6099.

[14] a) R. Rao, N. Pierce, D. Liptak, D. Hooper, G. Sargent, S. L. Semiatin, S. Curtarolo, A. R. Harutyunyan, B. Maruyama, *ACS Nano* **2013**, *7*, 1100; b) J.-M. Aguiar-Hualde, Y. Magnin, H. Amara, C. Bichara, *Carbon* **2017**, *120*, 226.

[15] X. Feng, S. W. Chee, R. Sharma, K. Liu, X. Xie, Q. Li, S. Fan, K. Jiang, *Nano Res.* **2011**, *4*, 767.

[16] a) A. Gorbunov, O. Jost, W. Pompe, A. Graff, *Appl. Surf. Sci.* **2002**, *197–198*, 563; b) S. V. Bulyarskiy, E. P. Kitsyuk, A. V. Lakalin, A. A. Pavlov, R. M. Ryazanov, *Russ. Microlectron.* **2020**, *49*, 25; c) S. Forel, A. Castan, H. Amara, I. Florea, F. Fossard, L. Catala, C. Bichara, T. Mallah, V. Huc, A. Loiseau, C.-S. Cojocaru, *Nanoscale* **2019**, *11*, 4091.

[17] H. Ago, N. Ishigami, N. Yoshihara, K. Imamoto, S. Akita, K.-i. Ikeda, M. Tsuji, T. Ikuta, K. Takahashi, *J. Phys. Chem. C* **2007**, *112*, 1735.

[18] a) Z. Tian, C. Wang, J. Yue, X. Zhang, L. Ma, *Catal. Sci. Technol.* **2019**, *9*, 2728; b) V. P. Santos, T. A. Wezendonk, J. J. D. Jaen, A. I. Dugulan, M. A. Nasalevich, H.-U. Islam, A. Chojecki, S. Sartipi, X. Sun, A. A. Hakeem, A. C. J. Koeken, M. Ruitenbeek, T. Davidian, G. R. Meima, G. Sankar, F. Kapteijn, M. Makkee, J. Gascon, *Nat. Commun.* **2015**, *6*, 6451; c) C. Yang, H. Zhao, Y. Hou, D. Ma, *J. Am. Chem. Soc.* **2012**, *134*, 15814.

[19] a) I. N. Shabanova, V. A. Trapeznikov, *J. Electron Spectrosc. Relat. Phenom.* **1975**, *6*, 297; b) E. de Smit, B. M. Weckhuysen, *Chem. Soc. Rev.* **2008**, *37*, 2758.

[20] a) L. Kang, S. Zhang, Q. Li, J. Zhang, *J. Am. Chem. Soc.* **2016**, *138*, 6727; b) J. Si, D. Zhong, H. Xu, M. Xiao, C. Yu, Z. Zhang, L.-M. Peng, *ACS Nano* **2018**, *12*, 627.